Field Testing of High Current Electrokinetic Nanoparticle Treatment for Corrosion Mitigation in Reinforced Concrete

Henry Cardenas[1], Joshua Alexander[1], Kunal Kupwade-Patil[1] and Luz Marina Calle[2]

[1]Applied Electrokinetics Laboratory (AEL), Louisiana Tech University, Ruston, Louisiana 71272, USA. E-mail: cardenas@latech.edu, *jba036@latech.edu*, *kvk001@latech.edu*

[2] Corrosion Technology Laboratory, NASA, Kennedy Space Center, Florida, 32899, USA. E-mail: luz.m.calle@nasa.gov

ABSTRACT

Electrokinetic Nanoparticle (EN) treatment was used as a rapid repair measure to mitigate chloride induced corrosion of reinforced concrete in the field. EN treatment uses an electric field to transport positively charged nanoparticles to the reinforcement through the concrete capillary pores. Cylindrical reinforced concrete specimens were batched with 4.5 wt % salt content (based on cement mass). Three distinct electrokinetic treatments were conducted using high current density (up to 5 A/m^2) to form a chloride penetration barrier that was established in 5 days, as opposed to the traditional 6-8 weeks, generally required for electrochemical chloride extraction (ECE). These treatments included basic EN treatment, EN with additional calcium treatment, and basic ECE treatment. Field exposures were conducted at the NASA Beachside Corrosion Test Site, Kennedy Space Center, Florida, USA. The specimens were subjected to sea water immersion at the test site as a post-treatment exposure. Following a 30-day post-treatment exposure period, the specimens were subjected to indirect tensile testing to evaluate treatment impact. The EN treated specimens exhibited 60% and 30% increases in tensile strength as compared to the untreated controls and ECE treated specimens respectively. The surfaces of the reinforcement bars of the control specimens were 67% covered by corrosion products. In contrast, the EN treated specimens exhibited corrosion coverage of only 4%. Scanning electron microscopy (SEM) revealed a dense concrete microstructure adjacent to the bars of the treated specimens as compared to the control and ECE specimens. Energy dispersive spectroscopic (EDS) analysis of the polished EN treated specimens showed a reduction in chloride content by a factor of 20 adjacent to the bars. This study demonstrated that EN treatment was successful in forming a chloride penetration barrier rapidly. This work also showed that the chloride barrier was effective when samples were exposed to field conditions at one of the most severely corrosive environments in North America.

INTRODUCTION

In 2001, the U.S. Federal Highway Administration in concert with CC Technologies Laboratories Inc., finalized a landmark study on the direct costs of corrosion in nearly every major U.S. industrial sector (Koch et al., 2002). Corrosion in bridge structures is an especially costly problem. The study found that the annual direct cost of highway bridge repairs (largely related to reinforcement corrosion) was $8.3 billion in the U.S. alone. The electrokinetic approach may provide an increase in the durability of concrete repairs by removing aggressive chemical species and sealing the region with a close chemical relative of the original cement binder material that is found in ordinary Portland cement. Figure 1 contains a schematic representation of a treatment applied to reinforced concrete. Such a treatment is expected to provide a sound foundation for application of traditional repair

materials that would otherwise be undermined by continued reinforcement corrosion. Unlike a typical coating, pozzolanic nanoparticles penetrate almost as deeply as desired with a minimal electric field as small as 1 volt/inch and a current draw as low as 0.1 ampere per square foot. Conventional coatings and topical repairs do not provide this efficiency since they must be applied evenly over the entire surface to ensure coverage.

Prior work examined the use of 24-nm, positively charged silica particles, for EN treatments in which the steel reinforcement was used as the cathode (Cardenas and Kupwade-Patil, 2007). In this treatment, the positively charged particles were drawn directly to the reinforcement while chloride ions were being driven away. The objective was to develop a chemical and structural corrosion barrier around the reinforcement. Initially, the treatment drew sodium, potassium, and calcium ions to the reinforcement surface, increasing the local alkalinity while driving away chlorides. Later, as the nanoparticles arrived, they were expected to react with available calcium to form a calcium-silicate-hydrate (C-S-H) barrier around the realkalized region. Additional particle loading was provided to fortify this physical barrier as more calcium became available further back from the reinforcement. The intention was that the physical barrier would "keep" the alkali metals close to the reinforcement while slowing/preventing the return of chlorides or other aggressive species. In re-exposure testing that followed treatment, the treated specimens showed little damage while the untreated controls were severely corroded.

The present work considered the use of elevated current density in order to accelerate the overall treatment process. Another feature of this work was the exposure to actual seawater at NASA's Beachside Corrosion Test Site, one of the most aggressive environments in North America.

EXPERIMENTAL PROCEDURE

This work focused on nanoparticle treatments using high current densities on 3 inch × 6 inch concrete test cylinders.

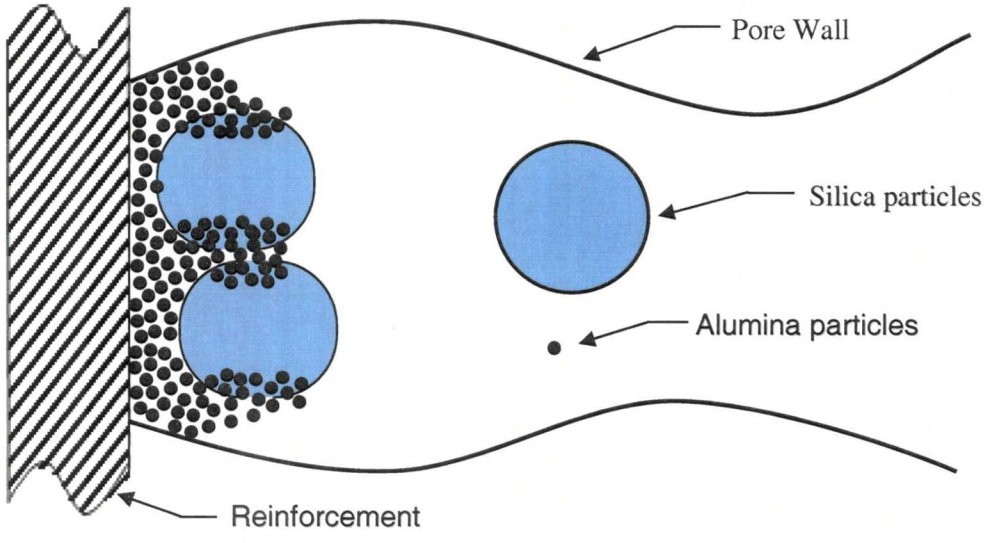

Fig 1. Predicted Formation of Particles in Cement Matrix after Treatment

The nanoparticle chosen for the treatment was a 24-nm diameter alumina coated silica particle. The 30 weight percent nanoparticle suspension was provided by Nalco Chemical, Naperville, IL, USA.

The mix design was completed as per ACI 211.1, for selecting proportions for normal, heavyweight and mass concrete. The mix ingredients in this case were Type I Portland cement, aggregate, water, and salt as shown in Table 1. The steel reinforcement inside the concrete was a 6-inch 1018 mild steel with a 0.25 inch diameter. The rebar was positioned in the center of the top of the specimen and embedded 3 inches into the concrete. The material was poured into the molds in three-volume increments as per ASTM C192.

Table 1. Batch Composition

Materials	Weight (lbs)
Water	18.5
Cement	36.5
Gravel	93.5
Sand	56.5
Salt	0.83

The purpose of this research was to investigate if it was possible to deliver the nanoparticles into the pores of the concrete using a high current without reducing the strength of the concrete. This hypothesis was tested by setting the power supplies to produce a voltage drop across each specimen of 25 volts per inch of cover. In this case, there was 1.5 inches of cover so the desired voltage drop for one specimen needed to be 37.5 volts. Also, the current was checked daily during treatment to ensure that a current density of 10 A/m^2 was not exceeded. Three different treatment solutions were compared in this work: EN, EN + Ca, and ECE.

One style of treatment involved connecting the specimens in series. This was accomplished by connecting two specimens per power supply (one EN and one ECE) and setting the power supply to produce a 37.5 volt drop across the EN-treated specimens. The circuit was connected so that the mixed metal oxide coated titanium counter electrode of one specimen was connected to the positive terminal of the power supply and the working electrode of the second specimen was connected to the negative terminal of the power supply. Figure 2 shows the circuit diagram for specimens connected in series. The treatment of each specimen was completed in a 4 inch × 8 inch plastic mold. A mixed metal oxide coated titanium electrode was formed in a helical fashion around the inside of the treatment container.

The second treatment type used in this work involved connecting the specimens in parallel. The same parameters as in the series treatment type were used for the parallel treatment type. The power supplies were set to produce a voltage drop of 37.5 volts across the specimens and the current was checked as to not exceed 5 A per square meter of concrete surface area. In this case, all of the specimens that were receiving similar treatments were placed in one container rather than each specimen having its own container. Similar to the series treatment setup, a titanium counter electrode was used to electrically push the nanoparticles into the pores of the concrete. Instead of the electrode going around the outside of the specimen, the electrode was placed in the center of the container and the specimens were organized around the electrode. Figure 3 shows the circuit diagram for the parallel setup.

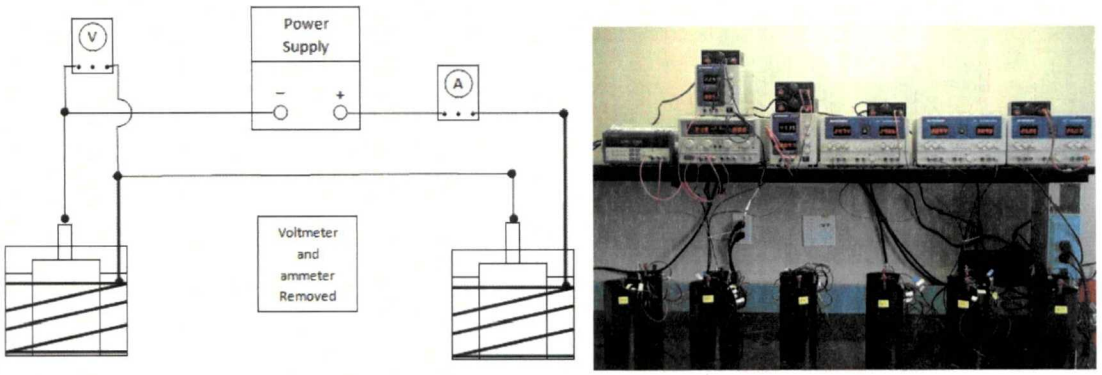

Fig 2. Treatment of Twelve Specimens Conducted in Series

All of the EN and EN + Ca treatment specimens started out in one container since both received similar treatments for the first 4 days. After the fourth day, the EN treatment specimens and EN + Ca treatment specimens were placed in different containers due to differences in the remaining treatment periods. After the fourth day of treatment, the EN specimens were separated from the EN + Ca specimens. The treatment solution on the fourth day for the EN specimens consisted of 0.16 L of nanoparticle solution and 4.16 L of deionized water. The treatment solution for the EN + Ca specimens consisted of 217 g of tetra flake calcium chloride (Tetra Technologies, The Woodland, TX) dissolved in 4.31 L of deionized water.

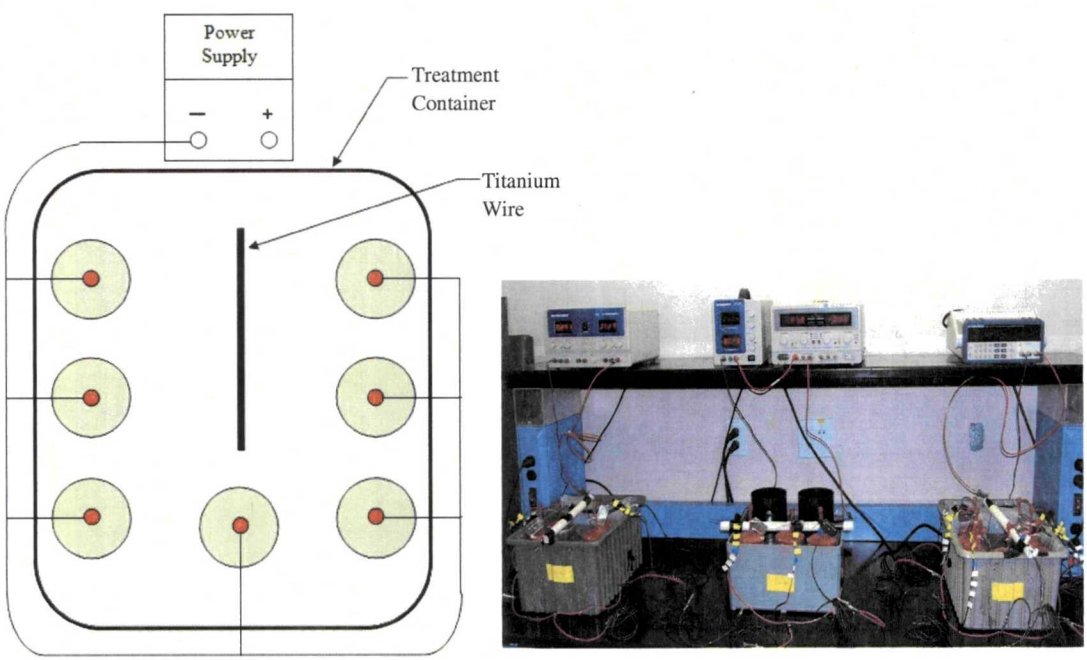

Fig 3. Treatment Setup Showing Specimens Arranged in a Parallel Treatment Circuit

Microscopic imaging samples were extracted from the broken concrete cylinders and vacuum mounted in epoxy. Polishing was conducted using 60, 120, 150, 320 and 600 grit size papers with the model Alpha-Beta Polisher manufactured by Buehler, Lake Bluff, IL. Micro-polishing was conducted with Buehler polishing-cloths ranging from 3-0.02 μm. These cloths were the ULTRA-PAD: 3 μm (for SiC removal), TEXMET 2000: 3 μm (for profile flattening), TRIDENT: 1 μm (for polishing), and the MICROCLOTH: 0.02 μm (for finishing). Polishing was conducted with a non-aqueous lubricant (propylene glycol) and with no particulate abrasives. After each polishing stage, the specimens were rinsed with ethyl alcohol to remove loose material. Microstructural analysis was conducted using a Hitachi S-4800 field emission scanning electron microscope (FE SEM) manufactured by Hitachi, Pleasanton, CA. Quantitative elemental analysis was done using the FE SEM Energy Dispersive Spectrum Analysis (EDAX) with Genesis Microanalysis software from Ametek Inc., Paoli, PA. Fourier transform infrared spectroscopy (FTIR) was conducted using a Mattson Genesis II FTIR spectrometer, manufactured by Mattson Genesis Inc., Middleton, WI. Samples were ground sufficiently to pass a No. 30 sieve and mixed with potassium bromide (KBr) in a ratio of 1:100. The mixture was compacted to provide a smooth test surface and pressed into pellets for transmittance measurements.

RESULTS AND DISCUSSION

The left side of Figure 4 contains a bar chart illustrating the measured surface areas that were covered with corrosion products. Each column represents a specific test category. Four to six specimens were tested in each of these categories. The value reported for each column is an average of these specimens. The first column on the left represents the controls examined just prior to treatment application. The 3% corrosion coverage occurred over a 21-day exposure period that preceded treatment. The remaining columns represent specimens that were tested following EN treatment and a 30-day post-treatment exposure to seawater. The EN-treated specimens exhibited 6% average corrosion coverage while the EN + Ca case revealed 4% average corrosion coverage. The specimens subjected to chloride extraction without particle treatment exhibited an 11% area of corrosion coverage. The control specimens were not subjected to any treatment. These exhibited an average corrosion area coverage of 67%.

The right side of Figure 4 shows a comparison of corrosion product coverage observed in each test case. Each specimen shown on the right side of Figure 5 represents the worst case observed in each category. The control specimen exhibited 67% corrosion coverage and showed evidence of pitting. The ECE specimen exhibited extensive corrosion damage with some pitting. The EN and EN + Ca specimens also exhibited some corrosion.

The specimens subjected to ECE treatment showed more corrosion when compared to the two EN treatment cases. The difference in corrosion coverage between both of the EN treated cases and the control specimens was also evident. In comparing these post-treatment cases to the pre-treatment specimens it was apparent that the controls and the ECE cases (Figure 4) exhibited more severe corrosion than the pre-treatment controls. The distinction between the two EN cases and the pretreatment controls was not readily apparent. This suggested that the EN and EN + calcium treatments kept the corrosion from progressing much beyond the original damage caused by the pre-treatment exposure. These visual observations appeared to reflect the same order of severity that is observed in the bar chart of Figure 4.

The ECE specimens and controls clearly exhibited the worst corrosion damage. These observations indicated that the EN and ECE treatments appeared to halt the corrosion

progress. The EN + Ca treatments did not appear to standout from the EN treatment. Perhaps a longer exposure period could possibly show differences in performance among these cases

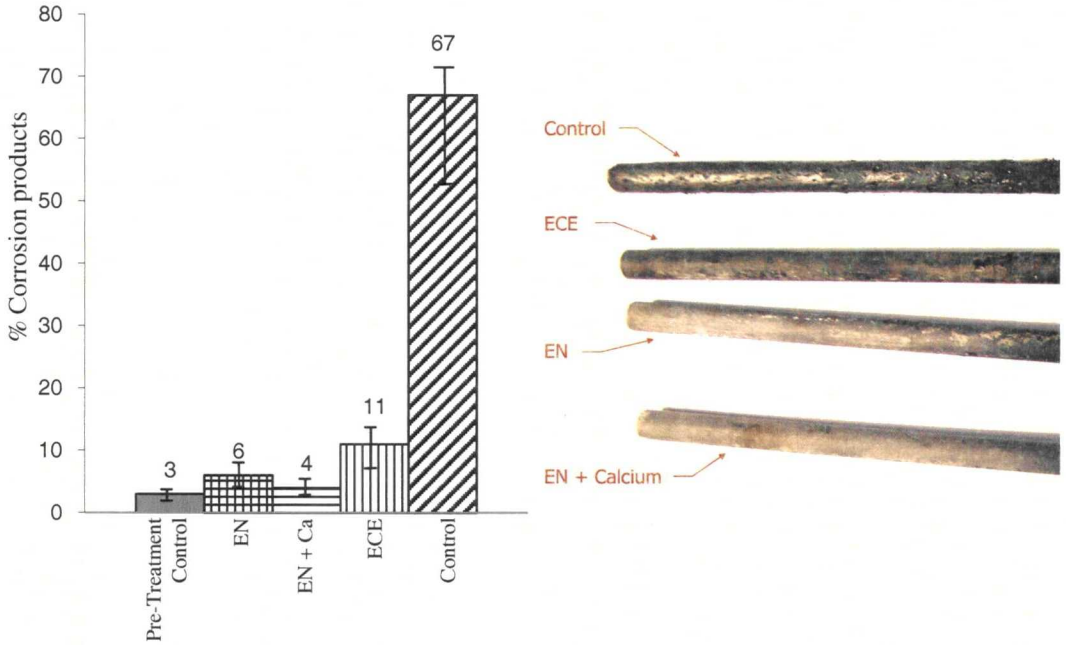

Fig 4. Corrosion Analysis that Compares the Measured Area Covered With Corrosion Products for Each Case

The results of the tensile and porosity tests carried out are illustrated in the bar chart of Figure 5. The EN + Ca and the ECE-treated specimens exhibited values of 221 and 219 psi respectively. The lowest strength values were observed among the untreated controls. These values were over 30% below the values obtained for the EN-treated specimens. EN treated and EN+ Ca treated cases exhibited 35% and 29% increases in strength as compared to the untreated controls. Reductions in porosity induced by particle treatments appeared to provide enhanced strength.

From Figure 5 it is clear that the EN-treated specimens were significantly stronger in tension than the untreated controls. This strength enhancement has two likely sources. The first source is the porosity reduction due to EN-treatment. In addition, the more extensive corrosion damage observed on the surfaces of the control specimens could have contributed to the lower strength result since the buildup of corrosion products on the bars could have caused the development of tensile residual stresses. This stress may have added to the stress present during the course of tensile testing, leading to a lower apparent strength.

The microstructure of these specimens was examined following tensile strength testing. Figure 6 provides a comparison in microstructure of the EN-treated and ECE-treated cases. The ECE-treated specimen appears to exhibit a typical porous morphology for fractured cement paste. The EN specimen image contains a fairly dense aggregate particle evident in 75% of the image. The upper left quadrant appears to contain cement paste. The morphology of this paste appears to be denser than that observed in the ECE case. A more extensive example of this densified morphology is exhibited in Figure 7. These samples were removed from a specimen subjected to EN treatment for 4 days followed by 3 days of calcium treatment. Both images clearly show the light-colored florets of a calcium-rich phase. The right side image also provides a clearer view of the densified cement morphology that is

typical of EN treatment. As shown in the chart in Figure 5, the calcium contribution did not appear to enhance the strength of the cylinders as compared to the EN treatment alone. The distance that all of these SEM samples resided from the steel reinforcement was approximately 1 mm. Based on the dosages of the treatments applied, the extent of the treated zone would be expected to range as much as 12 to 25 millimeter (mm) from the steel. It is thus not surprising that the SEM image of the EN treated specimen would exhibit a densified morphology at a distance of 1 mm from the steel.

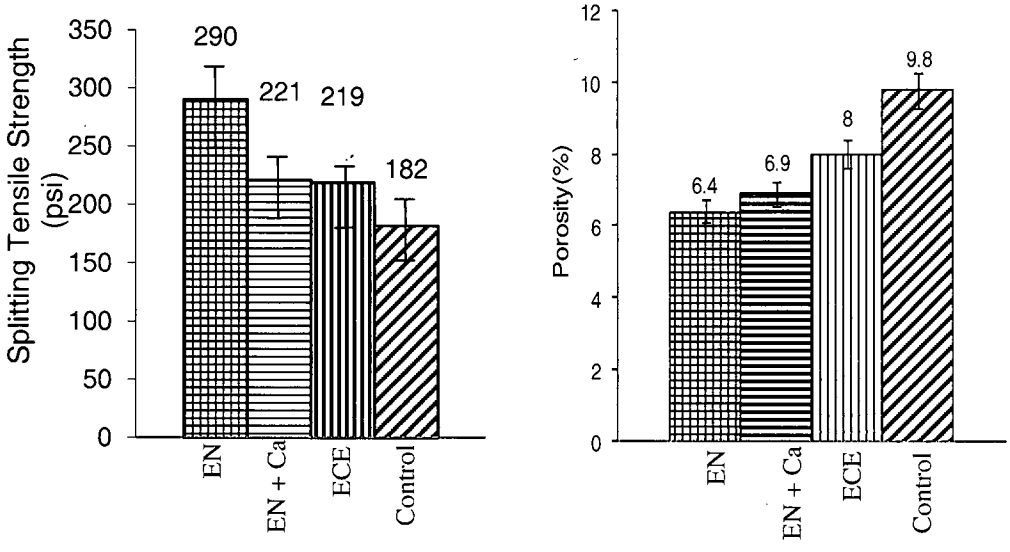

Fig 5. Comparison of Splitting Tensile Strength (Left) and Porosity (Right) for each Treatment Case

In Figure 5, the differences in tensile strength observed in these cases was not significant. The approximately 25% difference in strength between ECE and EN cases was notable. As indicated by the SEM images of Figures 6 and 7, the most likely cause for this strength increase was a porosity reduction due to nanoparticle loading of the capillary pore network in the concrete Each of the treatments shared chloride extraction as a common feature. In the cases of the nanoparticle treatments, the transport of particles going in and chlorides coming out was designed to be simultaneous. The question of chloride content was examined by Energy Dispersive X-Ray Spectroscopy (EDS) analysis of polished SEM specimens.

Figures 8 and 9 contain SEM images of EN treated and EN + Ca treated specimens after they had been re-immersed in saltwater for 30 days. The images exhibit relatively dark regions of aggregate surrounded by lighter regions of hardened cement paste. Occasional black areas are large pores or voids. In some cases, a particle of concrete became lodged in these pores (as indicated by a lighter color within them). EDS analysis was conducted on these polished surfaces in order to obtain quantitative information on the elemental content of the microstructures. The chart of peaks indicating the presence of various species appears to the right of each polished image.

Table 2 contains the chemical analysis results obtained from specimens representing each trial category of this study. It was observed that the controls exhibited the most sodium and chloride. The two EN cases exhibited the most aluminum. The EN + Ca cases exhibited the

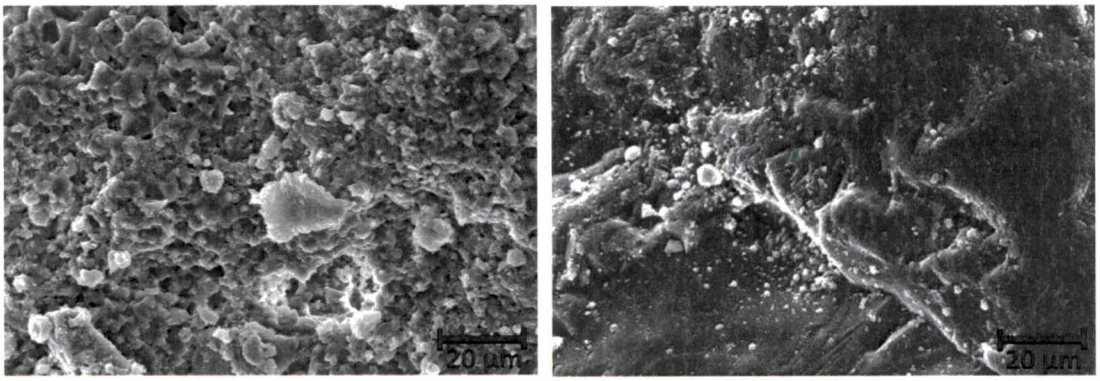

Fig 6. SEM Images of ECE and EN Specimens at a Distance of 1 mm from the Steel Reinforcement

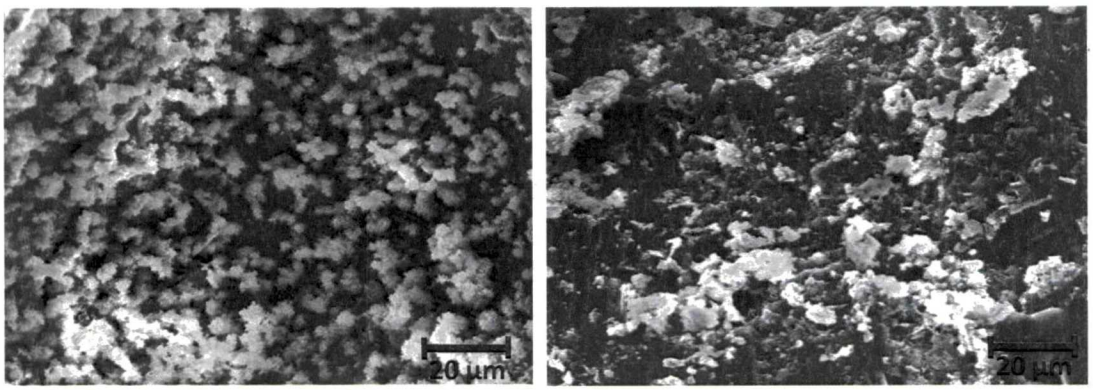

Fig 7. SEM Image of EN + Ca Treated Specimen Showing Light- Colored Calcium-Rich Deposits (Samples Taken 1 mm from the Steel Reinforcement)

highest calcium content. The highest silicon content observed was in the controls category. Of all the species listed in Table 2, the only ones that are not common to concrete are the sodium and chloride. The elevated sodium and chloride content of the controls is not surprising since these species are dominant in saltwater and there was no pore-blocking treatment applied in these cases that could stop the ingress of these species.

Table 2. Elemental Composition Results from SEM/EDAX Analysis

Specimen Type	Cl	Na	Al	Ca	Si
Controls	4.1	3.2	1.0	10.9	23.8
EN	0.0	0.3	1.1	14.8	10.0
EN + Ca	0.4	0.5	1.7	23.7	5.6
ECE	0.8	0.5	0.6	8.5	1.0

It is interesting to note that none of the cases exhibited an unusually high aluminum content. Alumina-coated silica particles carry a small amount of alumina. The calcium content was

understandably elevated in the EN + Ca case. The silicon content results are somewhat puzzling. The silicon content in hardened cement paste and many aggregates is expected to be reasonably significant. EN treatment would be expected to provide additional silicon but this value was decidedly smaller for the two EN cases 10 and 5.6 weight percent as compared to the 23.8 weight percent content of the untreated control. The near-zero silicon content of the ECE case is also puzzling.

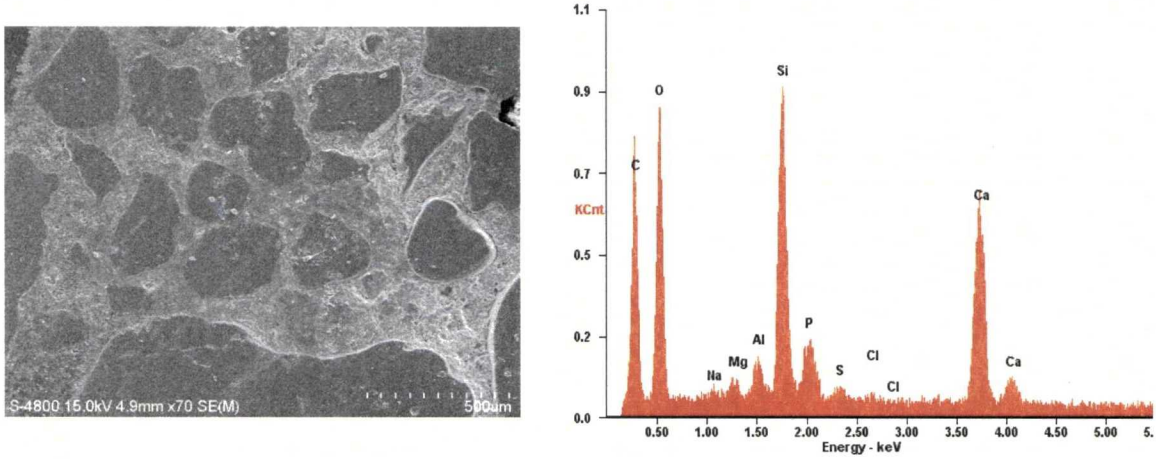

Fig 8. SEM Image of Polished EN Treated Concrete Specimen (Left) and EDS Analysis (Right).

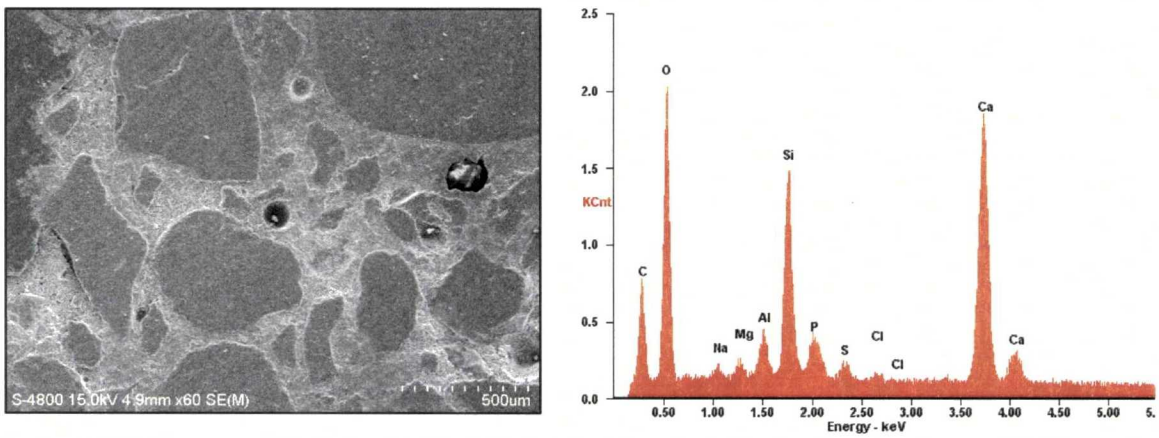

Fig 9. SEM Image of Polished EN + Calcium Treated Concrete Specimen (Left) and EDS Analysis (Right).

Table 3 contains a list of corrosion rates obtained from several control specimens subjected to saltwater immersion. The average value from this set is 0.41 mils per year (mpy). These values were obtained just prior to the initiation of treatments. Table 4 contains corrosion rates measured after the initiation of EN and ECE treatments. As compared to the pretreatment values, the corrosion rates after 1 day of treatment were generally over 200% higher than the pretreatment values. On the 4th day following the start of EN treatment, the corrosion rates were further increased. The corrosion rates for the EN and EN + Ca cases were 30% and 40% lower on average than those obtained on day 1. By day 7, these rates were 200% and 270% higher respectively.

The increase in corrosion rate observed after day 1 for all cases may have been due to the collection of positively charged ions at the electrode. These ions (typical of concrete) include silicon, calcium, and potassium. Under these circumstances, the coated electrode behaves as a rapidly corroding material in which the products of corrosion are various oxidation states of sodium, potassium, and calcium. Each time the EN or ECE treatment was paused, these species formed the basis of a rapid corrosion current. Thus, while the electrode is corroding, the products of corrosion do not necessarily include iron. Interestingly, by day 4 the corrosion rates for the EN cases dropped while those for the ECE cases rose. At the same time, it was anticipated that the first nanoparticles would be expected to arrive at the electrode after 1 day of treatment. If the particles were able to block the access of chlorides, it is reasonable to expect that they could be used to block the dissolution of sodium, potassium, and calcium. This may explain why the apparent corrosion rate drops off by day 4 in these cases while the ECE case exhibited a 16% increase. By day 7, the nanoparticles had long since arrived. Other arrivals may simply be additional ions that are falling in behind the nanoparticle layer. These new species layers could be providing the high-corrosion rates as they too come back off the now layered chemistry of the rebar surface.

Table 3. Corrosion Rates Measured During Treatment Period

Treatment Type	Corrosion rate after 1 Day (mpy*)	Corrosion rate change, Day 4 (%)	Corrosion rate change, Day 7 (%)
EN	1.34	-30	+200
EN + Ca	1.73	-41	+270
ECE	1.80	+16	+340

*mpy = mils per year

Fourier transform infrared (FTIR) spectra are shown in Figure 10. The spectra of the EN treated and EN + Ca samples exhibited peaks of tricalcium silicate (C_3S) at 867 cm^{-1}, calcium silicate hydrate (C-S-H) at 1100 cm^{-1} and calcium aluminate hydrate (C-A-H) in the range of 3400-3600 cm^{-1}. The presence of unreacted C_3S is not surprising since an 80-90% degree of hydration would have been reached by the time the specimens were sampled. The lack of C_3S in the controls may stem from the fact that they remained in outdoor exposure while the treated specimens were retained in lab conditions during the given treatment processes. The controls had the best chance of converting enough C_3S to prevent detection. It is unclear why the control sample exhibited no peaks associated with C-S-H.

A strong peak of C-S-H was observed in the mixture precipitate of alumina coated silica combined with simulated pore fluid (SPF). This particle also yielded another strength enhancing phase, C-A-H, which appears in Figure 10 in the range of 3400-3600 cm^{-1}. The mixture precipitate of colloidal alumina with SPF also exhibited a broad peak of C-A-H. Based on these observations, it appears that the increase in tensile strength among the EN and EN + Ca cases may be associated with the reaction of the nanoparticles with calcium hydroxide, leading to strength enhancing phases.

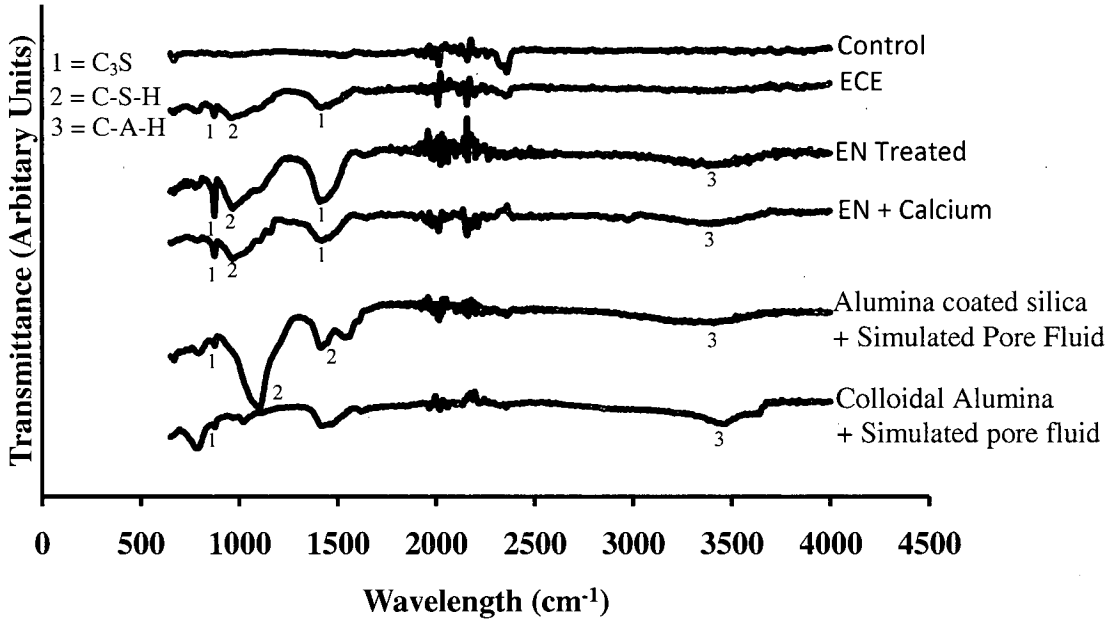

Fig 10. FTIR spectra of powdered specimens indicating C-S-H and C-A-H

CONCLUSIONS

The nanoparticle treatments were successful in reducing corrosion damage to the steel reinforcement in concrete after it had already started. These observations indicate that EN treatment, with and without the calcium post-treatments, were effective in stopping the return migration of chlorides.

The EN-treated specimens were significantly (25%– 30%) stronger in tension than the untreated controls. This strength enhancement had two likely sources. The first source was the porosity reduction due to EN treatment. The second source was the more extensive corrosion damage observed on the steel surfaces of the control specimens. These oxide phases could have contributed to the lower peak stress result for the controls since the buildup of corrosion products on the bars could have caused the development of tensile residual stresses, leading to a lower apparent strength.

The elevated sodium and chloride content of the untreated controls was not surprising since these species are dominant in saltwater and there was no pore-blocking treatment applied in these cases that could stop the ingress of sodium and chloride.

REFERENCES

ASTM C 78-02, "Standard test method for flexural strength of concrete (using simple beam with three-point loading)", American society of testing and materials, Philadelphia, 2002.
ASTM C 496-96, "Standard test method for splitting tensile strength of cylindrical concrete specimens", American society of testing and materials, Philadelphia, 2002.
ASTM C 876-91, "Standard test method for half cell potentials of uncoated reinforcing steel in concrete," American society of testing and materials, Philadelphia, 2002.

ASTM G3-89, "Standard practice for conventions applicable to electrochemical measurements in corrosion testing," American society of testing and materials, Philadelphia, 2002.
ASTM C 900-01, "Standard test method for pullout strength of hardened concrete", American society of testing and materials, Philadelphia, 2002.
ASTM C 1152., "Standard test method for acid- soluble chloride in mortar and concrete", American society of testing and materials, Philadelphia, 2002.
ASTM G109, "Standard test method for determining the effects of chemical admixtures on the corrosion of embedded steel reinforcement in concrete exposed to chloride environments", American society of testing and materials, Philadelphia, 2002.
Bentur , A., Diamond, S., and Berke, N. "Steel corrosion in concrete", E & FN Spon, London, UK, 1997.
Mays, G. (1992). *Durability of Concrete Structure: Investigation, Repair, Protection,* 1st Ed, E & FN Spon, London.
Broomfield, J. (1997). *Corrosion of Steel in Concrete, Understring, Investigation and Repair,* 1st Ed, E & FN Spon, London.
Brown, M., Smith, C., Seller, G., Folliard, K., and Breen, J. "Use of alternative materials to reduce shrinkage cracking in bridge decks, " *ACI Materials Journal*, Vol. 104, Nov-Dec, 2007, pp. 629-637.
Fajardo, G., Escadellias, G., and Arliguie, G. "Electrochemical chloride extraction from steel reinforced concrete specimens contaminated by artificial sea water ," *Corrosion Science*, Vol. 48, Nov, 2004, pp. 110-125.
Cardenas, H., and Kupwade-Patil, K. "Corrosion Remediation using chloride extraction concurrent with electrokinetic pozzolan deposition in concrete," New solutions for environmental pollution, Proc. Intern. Symp on electrokinetic remediation, 12 – 15 June 2007, Vigo, pp. 117.
Cardenas, H., and Struble, L., "Electrokinetic nanoparticle treatment of hardened cement paste for reduction of permeability," *Journal of materials in civil engineering,* Vol.18, No.1, July-Aug, 2006, pp.554-560.
Johansen, V., Goltermann, P., Thaulow, N. "Chloride Transport in Concrete," *Concrete International*, Vol. 17, July, 1995, pp. 43-44.
Jones, A. D., "Principle and Prevention of Corrosion", Prentice Hall Inc., Upper Saddle River, 1995.
Kan, Y., Yen, T, and Lee, M. "Restored strength of cracked concrete beam repaired by Epoxy and Polymethyl Methacrylate," *ACI Materials Journal*, Vol 105, Sept-Oct, 2008, pp. 451- 458.
Koch, G. H., M. P. H. Brongers, Thompson, N. G., Virmani, Y. P., Payer, J. H., Corrosion Costs and Preventive Strategies in the United States, Publication No. FHWA-RD-O1-156, Materials Performance, National Association of Corrosion Engineers, July 2001, pp. 3-11.
Kupwade-Patil K, 2007, A new corrosion mitigation strategy using nanoscale pozzolan deposition, Master's thesis, Louisiana Tech University.
Kupwade-Patil, K and Cardenas, H. "Corrosion mitigation in concrete using electrokinetic injection of reactive composite nanoparticles," Society for the advancement of material and process engineering, 18-22 May, 2008, Long Beach, CA.
Kupwade-Patil, K., Gordan, K., Xu, K., Moral, O., Cardenas, H., and Lee, L. "Corrosion mitiagation in concrete beams using electrokinetic nanoparticle ," Excellence in concrete construction through innovation, 9-10 Sept, 2008, London, UK, pp.365-371.
Orellan, J.C, Escadellias, G., and Arliguie, G. "Electrochemical chloride extraction efficiency and side effects," *Cement and Concrete Research*, Vol. 34, Feb 2004, pp. 227-234.
Shi, M.; Chen, Z.; and Sun, J., 1999, "Determination of chloride diffusivity in concrete by AC Impedance spectroscopy," *Cement and Concrete Research,* V.29, pp.1111-1117.